2015 WJTA-IMCA Conference and Expo
November 2-4 ● New Orleans, Louisiana

Paper

DEVELOPMENT AND TESTING OF ULTRA-HIGH PRESSURE DOWNHOLE PUMP DRIVEN BY VANE MOTOR

Shi Huaizhong, Li Gensheng, Li Hao, Zhang Yi
State Key Laboratory of Petroleum Resources and Prospecting, China University of Petroleum Beijing, Beijing 102249, China

ABSTRACT

Ultra-high pressure, jet-assist drilling techniques proved to be an efficient way to increase rock breaking efficiency in deep wells where rocks become harder and more difficult to drill. In this technique, the ultra-high pressure down-hole pump, which locates between the drilling collar and the drilling bit, is the key component. This paper presents the development and testing for a novel ultra-high pressure and jet-assist down-hole pump using hemispherical vane motor. The mechanical principle is that when drilling mud flows through the vane motor from the inlet to the outlet, it causes pressure loss and pushes the rotor and the crankshaft and connecting rod mechanism to rotate at a high speed along the axis. The crankshaft and connecting rod drive the plunger to reciprocate back and forth in the pump. The mechanism of energy transform is to convert the kinetic energy of mud into the rotating speed mechanical energy. First, the shell, the vane motor assembly, the crankshaft and connecting rod mechanism, the plunger, and cylinder liner etc. are redesigned to meet the purpose of increasing the rock breaking efficiency. Second, a numerical simulation is built to better understanding the flow behaviors of the novel pump. Third, the torque of motor, pressure loss, motor structure, and vane size and numbers are studied using CFD technique. At last, intensive laboratory experiments are designed to test the hydraulic parameters of the novel pump. The results show that: 1) the rotor torque increases with the increase of drilling mud flow rate. 2) The torque of the vane motor assembly is up to 400 N·m and the outlet pressure of the pump is about 14Mpa when the flow rate is 14L/s.

1 INTRODUCTION

In 1993, FlowDril and Gas Research Institute (GRI) developed downhole ultra-high pressure pump to carry out jet-assisted rock breaking research plan (Veenhuizen 4-6), in which booster increases the pressure of some fluid to help drilling. The experimental result shows that ROP can be improved 1.0~2.5 times.

At the end of 1994, the U.S. Department of Energy (DOE), FlowDril and GRI jointly developed the second generation of downhole pump prototype (Veenhuizen, Stang, and Kelley 1-4). Field test results shows that jet-assisted drilling with ultra-high pressure downhole pump can increase rate of penetration by 45%~100%, while the device's working life is short.

In 2001, Maurer Engineering Inc. conducted the research and development of high-pressure jet drilling system, indoor experiment field test (Cohen and Deskins 2-8). The system can send BHA into borehole through coiled tubing and also use improved conventional rotary drilling methods. The indoor experiment shows that jet kerf drilling technique can improve ROP by 1.0~2.0 times in different formations. Field tests in a number of different formations including sandstone, shale, arenaceous shale, limestone, etc. indicate that the mechanical drilling rate can be improved by 1.3~6.0 times.

In 2003, Li et al. put forward hydraulic pulsed self-oscillation cavitation jet and studied the jet characteristics experimentally (Li, Shen, Zhou, Zhang, and Yi 570-75). The results shows that the impact pressure peak value and pulse amplitude of self-oscillation cavitation jet is 37% and 24% higher than ordinary nozzle, respectively.

In 2005, Wang et at. completed the design of the first generation of fluidic downhole pressure booster (Wang, Xue, and Zou 17-19). Ground simulation test and whole machine pilot of the device shows that outlet pressure changes directly associated with the input displacement and throttling pressure drop, and the pressure fluctuation of stand pipe also reflects that the designed tool's pressure loss conforms with the actual experimental pressure loss.

Guan et al. designed a novel downhole pressure booster using drilling string's vibration as energy source (Wei 67-80). The device can take advantage of the axial vibration which drives plunger piston to reciprocate up and down. In this way, vibration during drilling can be turned into beneficial reciprocating motion of the plunger, and thus drilling mud is compressed and the pressure is increased. This device not only alleviates drilling string's vibration but also boosts the drilling mud's pressure.

Predecessors did a lot of work in this area (Kolle 61-69; Dou 1-7 151; and Fu 5-11).On the basis of previous studies, this paper puts forward a novel downhole pressure pump driven by vane motor which uses drilling fluid to drive the vane, and crankshaft turns torque into piston's reciprocating movement to provide local high pressure jet-assisted rock breaking capacity. The novel pressure pump can provide new ideas for downhole pressured jet assisted rock breaking method.

2 STRUCTURE AND WORKING PRINCIPLE

2.1 Structure

Hemispherical vane motor mainly includes the following five parts: shell, separator, vane motor assembly, crank-link mechanism and plunger pump assembly. Its upper end can connect drill collar or PDM, and the lower end can directly connect drill bit. In the process of drilling, drilling fluid coming from drill collar or PDM passes through the separator located at the upper part of the pressure pump, and then most of the fluid goes into the high pressure inlet of a pair of vane motors. Therefore, under the effect of differential fluid pressure, the vanes generate torque and drive the rotor. The rotor makes the crankshaft rotate, which makes the connecting rod and plunger piston reciprocate up and down. In this way, a small part of the high pressure drilling fluid coming from collar or PDM turns into ultra-high pressure fluid, and the ultra-high pressure jet comes out of the ultra-high pressure nozzle and assists downhole rock breaking process to improve the ROP.

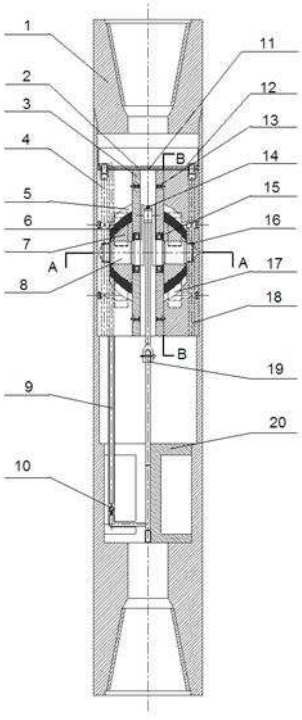

1. Body 2. Separator 3. Motor gland 4. Fluid inlet 5. Vanes 6.Spring 7. Rotor 8. Crank shaft 9. Channel 10. One-way valve 11. Spacer 12. Through-hole bolt 13. Gland bolt 14. Connecting rod and set bolt 15. Bearing and seal 16. Bearing bush 17. High pressure and low pressure chambers 18.Fluid outlet 19. Cardan shaft 20. Plunger pump

Figure 1. Structure of Downhole Pump Driven by Vane Motor

The Pump which drives the crank-link mechanism can continuously provide power for plunger pump and make ultra-high jet continuously act on the downhole. The structure is shown in Figure 1.

2.2 Working Principle

At the upper part of the downhole pump driven by vane motor there is a separator, which divides drilling fluid coming from drill collar or PDM into three parts, in which two parts of the fluid flows into the high pressure inlet section, and the third part goes into the plunger pump's inlet section through the channel opened at the motor stator.

A pair of symmetrical vane motors is mounted next to the separator under the limited downhole space and the stator's inside profile is semi-spherical. Two high pressure chambers and two low pressure chambers are installed at the motor stators. High pressure drilling fluid coming from the high pressure chambers flows into the low pressure chambers, so the pressure difference is produced driving rotor to rotate.

Spring is installed between vanes and rotor slot. When the vanes rotate to the position where the stator's inner diameter is the minimum, spring will be pressed thoroughly, while when the vanes reach the position where the inner diameter is the maximum, spring will push the vane's edge to the stator's inner surface. Sliding bearing, seal system and the crank-link mechanism are also designed according to the downhole space. The stators are installed on both ends of the crankshaft.

Plunger pump is located at the bottom and its main body sits on the shell. The drilling fluid at the inlet comes directly from the separator, and the outlet fluid flows through high pressure channel and moves out of bit nozzle to break rocks.

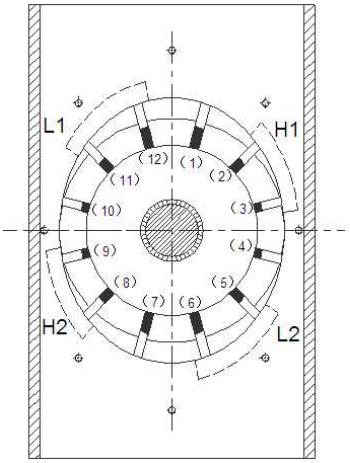

Figure 2. B-B Sectional View

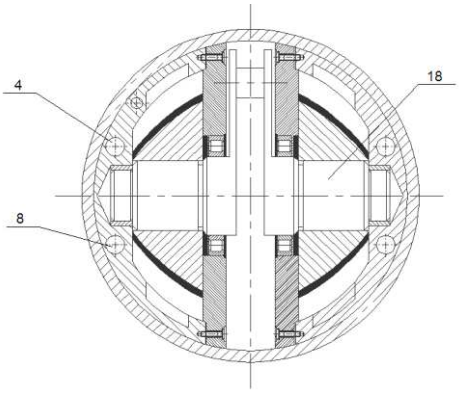

Figure 3. A-A Sectional View

The core section of the device is the vane motor, which can be more detailed observed from B-B and A-A sectional view. In the above figures, L1 and L2 indicate low pressure chambers; H1 and H2 indicate high pressure chambers.

3 NUMERICAL SIMULATION OF HYDRAULIC PARAMETER'S CHARACTERISTICS

Hemispherical vane motor is the key component of the whole device, and its structure is directly related to the energy transform efficiency of the pressure pump system, which is key to the design. This paper uses FLUENT software to study the hemispherical vane motor model. Similar numerical simulation and optimization for dwonhole boost compressor has been done (Wang 308-12; Xue 5-11; and Ai 92-4).

3.1 Geometric Model

Due to the symmetry of hemispherical vane motor, we only analyze the fluid flow of one vane. Each side of the motor has two inlets and two outlets, as shown in Figure 4. The blue section indicates velocity inlet and the red one indicates pressure outlet. The green part shows the shell and the grey one means the rotor. Since the top and bottom radii of actual motor are relatively small and contact seal is adopted between vane and shell, there is no space between top and bottom vanes during simulation and the space between vanes and shell on both sides is 1 mm. The rest of the parameters are of the same size as the actual test device.

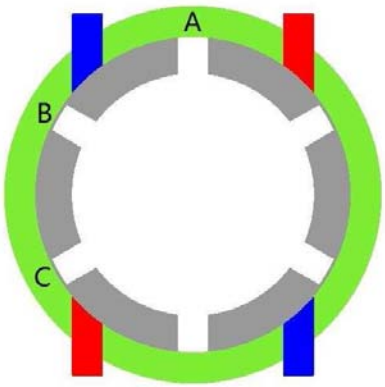

Figure 4. Two-dimensional Flow Model

RNG k-epsilon turbulence model is adopted due to the unsteady flow field. Unstructured mesh was used with the mesh size of 0.3, and the sliding mesh was adopted to simulate the rotation of the rotor in the stator.

3.2 Boundary Condition

Inlet boundary was set as velocity inlet; Outlet boundary was pressure outlet; Wall condition was set as stationary wall.

3.3 Sliding Mesh Settings

According to the measured data in practical experiment and the conditions in real operation, we assume the rotational speed of the rotor is 30 rpm (revolutions per minute). Between the two inlets and two outlets interfaces were set, and the space between vane and stator was 0 mm according to real design. Therefore, the rotation time that dynamic mesh can simulate is limited.

In the simulation, the velocity field that vane A rotates counterclockwise to the position 30° to the velocity inlet can be simulated. Due to the cyclic process of the whole vane's flow field, the flow field between this 30° can be used to speculate the pressure and torque during the whole rotation of vane motor.

3.4 Numerical Simulation Method

1. Flow rate

According to the flow rate of working condition, the inner flow fields of one side of the vane motor was simulated when the flow rate was 3L/s、5L/s、7L/s, respectively. The corresponding inlet velocities are shown in Table 1.

Table 1. Simulation Scheme of Different Velocities

Flow Rate(L/s)	3	5	7
Inlet Velocity(m/s)	4.3	7.1	10

2. Angle of rotation

When rotor rotates, the relative position among vane, inlet and outlet will change, which means the impact force will change accordingly. Analyzing the torque change at different angle of rotation can get the dependability of this tool.

3.5 Calculation and Analysis Results

3.5.1 Pressure Field Analysis

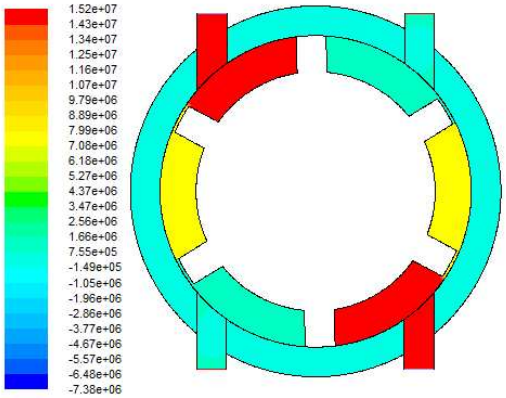

Figure 5. Pressure Field Distribution at the Beginning with Inlet Velocity of 10 m/s

Figure 5 is the pressure field of the vane motor with velocity of 10m/s at both inlets. In this figure, we can see that the pressure field of the vane motor is centrosymmetric and the pressure in channels on both sides attenuates from the inlet to outlet. Vane B and C provide torque for the whole vane motor and vane A in the real tool is compressed into the crank shaft of the vane motor, so when we calculate the torque, we don't take vane A into account. As shown in Figure 5, the pressure in space between vane A and B and vane B and C are respectively 15Mpa and 8Mpa, and the pressure at the outlet is 0.8Mpa.

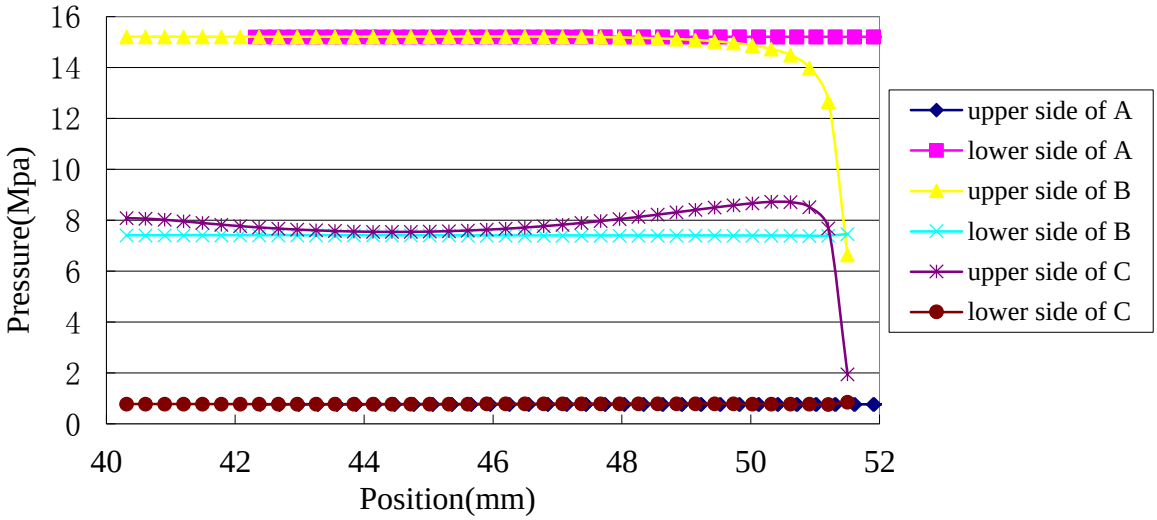

Figure 6. Pressure Distribution Curve for Different Vanes

Figure 6 shows the pressure curve of each vane on both upper and lower sides. As shown in Figure 6, the pressure on different sides of vane A shows great diversity, but in the real tool vane A does not generate torque. The pressure between two vanes have little difference on the upper side and the lower side. For example, the pressure on the lower side of vane B is approximately the same of that on the upper side of vane C. For vane B and C, the pressure shows a great decrease at the finger tip of the vane because the velocity at that point increases greatly.

3.5.2 Flow Field

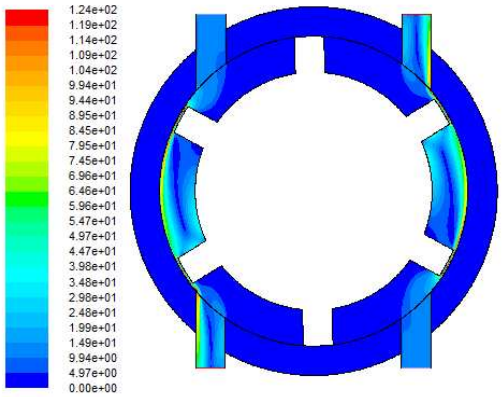

Figure 7. Flow Field with Inlet Velocity of 10 L/s and Gap of 1 mm

Figure 7 shows the flow field when fluid flows through the vane motor at velocity of 10m/s at initial moment. In this figure, we can see that since the gap between the vane and the stator is very small, velocity here is quite high—approximately 120m/s. What's more, the high-speed water flow impacts the vane of the motor and generates flow back at the upper side of each vane. At last, the fluid flows out of the outlet and the flow field is centrosymmetric.

3.5.3 Impact of the Inlet Velocity on Pressure Field and Torque

Keeping the rotational speed at 30rpm, the initial flow fields with inlet velocity of 4.3m/s, 7.1m/s and 10m/s were analyzed respectively. Since vane B and vane C generates most torque, taking vane as cantilever beam, the maximum torque can be calculated according to the differential relation between the load and the torque.

$$\frac{d^2M(x)}{dx^2} = \frac{dF_S(x)}{dx} = q(x) \tag{1}$$

Extracting data from both sides of vane B and vane C, torque map of the vane can be calculated by differential equation shown above. The torque map is shown in Figure 8.

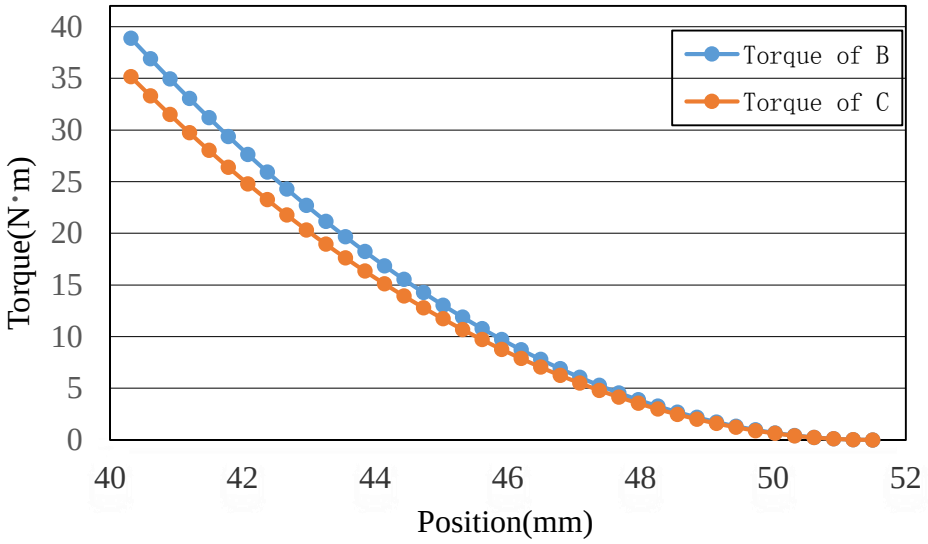

Figure 8. Torque Distribution Curve with Flow Rate of 10 m/s

As shown in Figure 8, the toque in both vanes increases from the finger tip to the root tip. The maximum torque provided by vane B and vane C are 40 N·m and 36 N·m, respectively. Since every side of the motor is centrosymmetric and one motor has a pair of vanes. The total torque is four times as much as the torque provided by vane A and vane B.

3.5.4 Torque at Different Rotation Angle

The rotation process of the motor is simulated to evaluate the motion state. As the motor rotates, the impact force will change. The torques of vane B and C at different position with inlet velocity of 10m/s is calculated respectively.

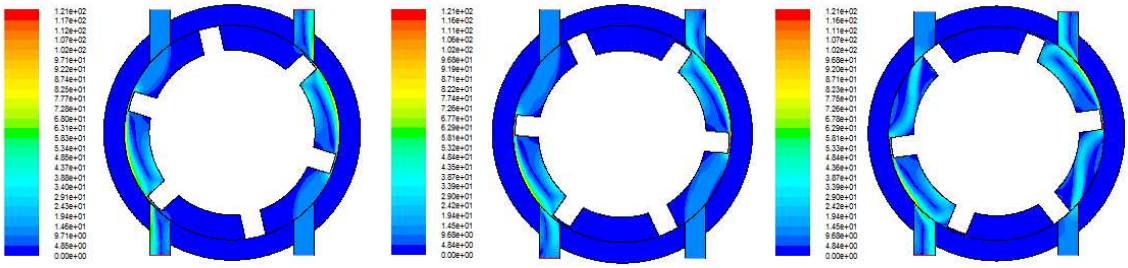

Figure 9. Fluid Field at 0.07s,0.14s and 0.21s

The figures above show the flow field at different rotation time. In these figures, we can see that the flow fields at different time have no obvious difference. At 0.21s, since vane A

obstructs the inlet, a relatively high speed water flow forms at the inlet.

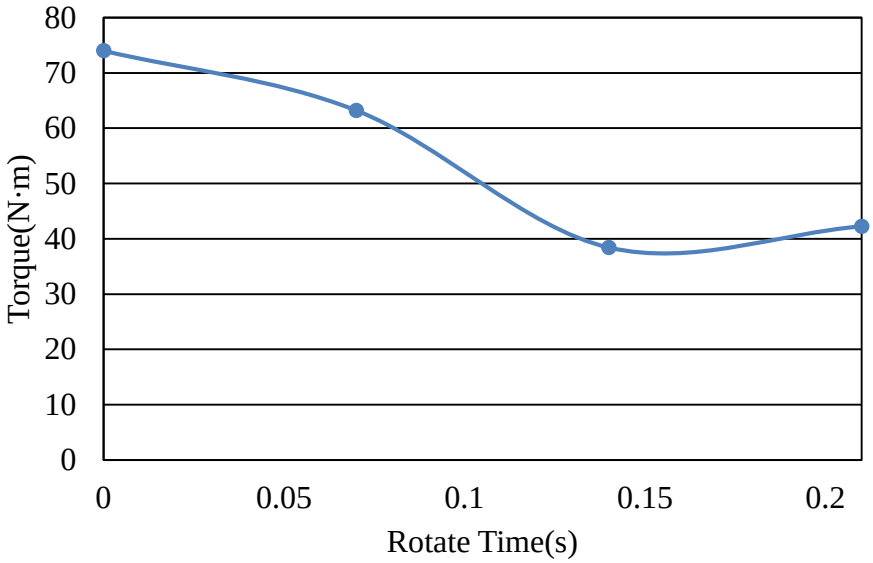

Figure 10. Torque Provided by Vane B and C at Different Rotate Time

The total torques of vane B and C at different rotation times are calculated and the results are shown in Figure 10. We can see that from the initial moment to 0.21s, the torque decreases from maximum 75N·m to 40N·m. This is mainly because vane C rotates across the outlet and the fluid impact on vane C decreases. The torque is provided mainly by vane B at 0.21s.

4 HYDRAULIC PARAMETER LABORATORY EXPERIMENT

4.1 Preparation

All components of the hemispherical vane motor are manufactured and assembled, and engine oil is used as the flow medium. Main components of the hemispherical vane motor are shown in Figure 11. The rotate speed and the torque generated by the motor are measured with the flow rate with one side of the motor changing from 3L/s-7L/s.

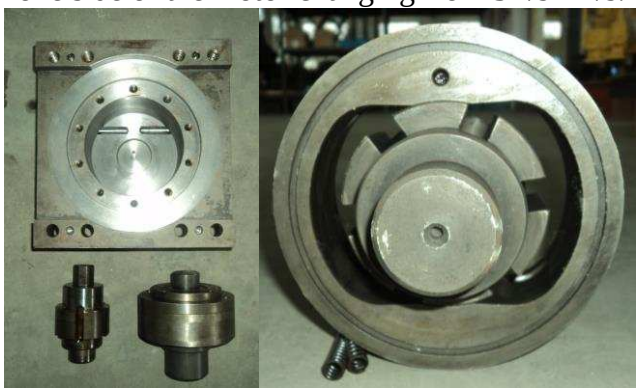

Figure 11. Hemispherical Vane Motor Components

The main components in Figure 11 are shell, stator, crank shaft. The stator, upper cover and lower cover are fitted together by pin bolt, creating a cavity with two inlets and two outlets. Crank shaft is placed inside the cavity with six retractable vanes fixed in it. These are the main components of the motor. The motor is fixed inside the shell by cover plate with its

flow pass connected to the corresponding flow pass of the shell. Then one side of the testing prototype is assembled. The two sides are totally symmetrical with crank shafts of two sides connected by hexagonal joint and shell connected with bolt.

4.2 Experimental Scheme

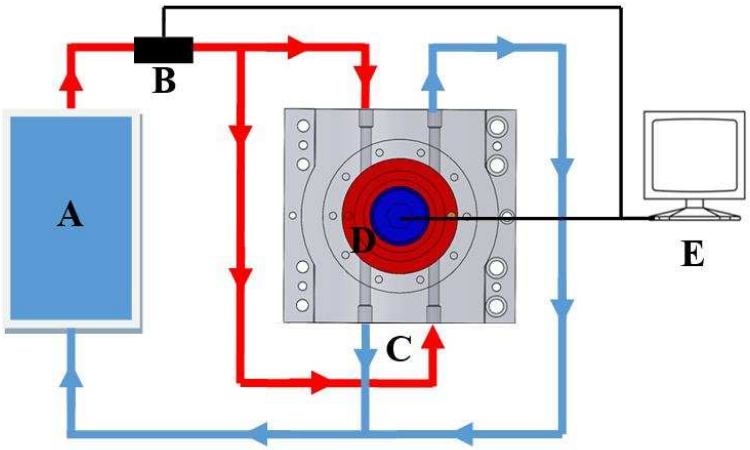

A Pump; B Pressure Transmitter; C Hemispherical Vane Motor Testing Prototype;
D Torque Measurement Device; E Data Acquisition System

Figure 12. Experimental Facilities Schematic Diagram

Figure 12 shows the schematic diagram of experimental facility. Pump A pumps engine oil out through the hose into the two inlets of the motor. Before the inlets a pressure sensor B is installed to measure the inlet pressure. Since a vane motor is composed of two identical sides, in this experiment only one side of the vane motor C is tested. The crank shaft is connected with torque measurement device D, which is connected to the computer E. Both pressure data and torque data can be gathered by computer. Real testing prototype is shown in Figure 13.

Figure 13. Hemispherical Vane Motor Testing Prototype Picture

4.3 Experiment Results

The inlet pressure, rotate rate and torque of the vane motor are measured and the results are shown in Figure 14.

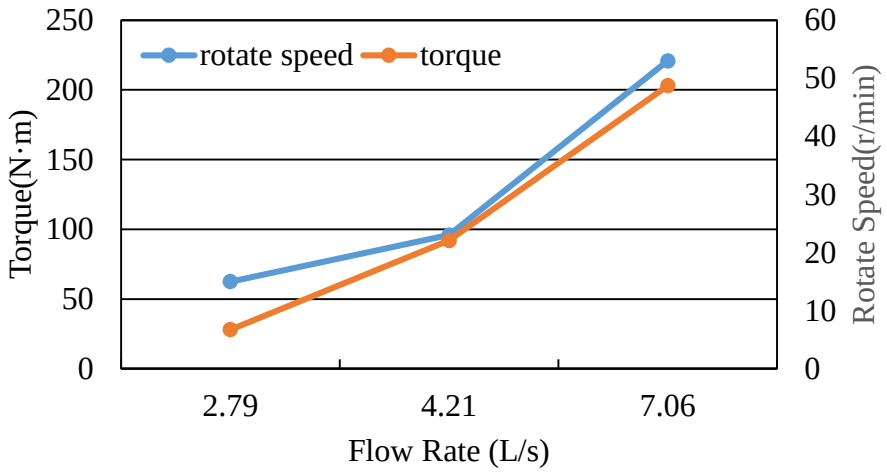

Figure 14. Test Result of One side of the Hemispherical Vane Motor

Test result and simulation result are basically unanimous and the value in test result is higher than simulation result. This is probably because in real test engine oil is used instead of water as the working fluid. What's more, the vane fixed in the crank shaft is retractable and can closely contact the inner wall of the motor.

Through the test, we find that this motor still need to be improved. By increasing the length of the vanes, more water energy can be transferred into kinetic energy of the motor. The parameter optimization needs further research.

5 CONCLUSIONS

In this paper, the structure and working principle of the novel pump driven by vane motor is illustrated. Through laboratory experiment and simulation, the inner flow field and working characteristics of this pump is studied. Through the above work, we come to the following conclusions.

1. A novel pump is designed and a testing prototype is manufactured. This novel pump prototype is proved feasible through laboratory experiment.

2. Through numerical simulation, the torque and the pressure loss provided by a single side of the motor are 150N·m and 14Mpa respectively. For vane B and C on a single side of the motor at the initial time, the torque provided by vane B is 40 N·m and that by vane C is 36 N·m. Moreover, when the motor rotates, the torque changes from 75N·m to 40N·m periodically.

3. In laboratory experiment, the torque and rotate speed at flow rate of 7L/s by a single side of the motor are 53rpm and 203 N·m. When flow rate is 4.21L/s and 2.79L/s, the test result shows that the rotate speed and the torque decrease as the flow rate decreases. The motor performs better in laboratory test than in numerical simulation.

4. The numerical simulation result and laboratory result show that downhole pump

driven by vane motor is feasible and this novel pump provides a novel method for ultra-high pressure jet-assist drilling technique.

6 ACKNOWLEDGEMENT

This work was part of the program on Investigation of Partial Underbalanced Drilling Hydraulic Characteristics modulated by Coiled Tubing funded under the national nature science foundation of China. The authors are grateful to all study participants.

REFERENCE

Ai, Chi, et al. "Calculating methods of principal structure parameters of diaphragm pressure converter." Journal of Daqing Petroleum Institute25.1 (2001) 92-94. Print.

Cohen, J H, and Deskins G. "High-pressure jet kerf drilling shows significant potential to increase ROP." SPE96557 (2005):2-8. Print.

Dou, Liangbin, et al. "Research progress on ultra－high pressure jet drilling by down－hole pressure boost." Special Oil & Gas Reservoirs3 (2012):1-7, 151. Print.

Fu, Jiasheng, et al. "Study on supercharging characteristic of downhole pulsed pressure intensified drilling device." China Petroleum Machinery1 (2015):5-11. Print.

Kolle, JJ, et al. "Development of a downhole separator and intensifier for coiled tubing jetting." Journal of Canadian Petroleum Technology47.12 (2008):61-69. Print.

Li, Gensheng, et al. "Mechanisms and tests for hydraulic pulsed cavitating jet assisted drilling." Petroleum Exploration and Development2 (2008):239-243. Print.

Li, Gensheng, et al. "An experimental study on impact pressure characteristics of self-resonant cavitating jets." Journal of Hydrodynamics (A)5 (2003):570-575. Print.

Li, Weicheng, et al. "Development and application of a new ultra-high pressure downhole supercharging system" Natural Gas Industry3 (2015):86-92. Print.

Sun, Wei, et al. "System design of the centrifugal downhole pressure device." China Petroleum Machinery34.3 (2006):36-38. Print.

Veenhuizen, S D. "Development and testing of a downhole pump for jet-assist drilling." Natural Gas RD&D Contractors Review Meeting (1995):4-6. Print.

Veenhuizen, S D, et al. "Development and testing of downhole pump for high-pressure jet-assist drilling." SPE38581 (1997):1-4. Print.

Wei, Wengzhong. "Study on vibration characteristic of bottom drilling string and design of drilling string shock absorption & downhole hydraulic pressurizing system." China University of Petroleum (Hua Dong) (2007):67-80. Print.

Wang, Zhiming, Xue Liang, and Zou Hejun. "Study of design theory of piston-type downhole booster." China Petroleum Machinery (2007):17-19. Print.

Wang, Zhiming, and Xue Liang. "Hydraulic parameter model for design of fluidics downhole boost compressor" Acta Petrolei Sinica29.2 (2008):308-312. Print.

Xue, Liang, Wang Zhiming, and Li Bangmin. "Numerical study of flow field for fluidic downhole boost compressor." Petroleum Drilling Technology1 (2015):5-11. Print.

Xu, Yi, et al. "Principle and design of screw downhole supercharger." Drilling and Production Technology34.3 (2011):71-73. Print.